Prediction of Flow Fields in a Dual-Impeller Stirred Vessel

Giorgio Micale, Alberto Brucato, and Franco Grisafi
Dipartimento di Ingegneria Chimica, Università di Palermo, Viale delle Scienze, 90128 Palermo, Italy

Michele Ciofalo
Dipartimento di Ingegneria Nucleare, Università di Palermo, Viale delle Scienze, 90128 Palermo, Italy

Numerical simulations were conducted for the flow field in a baffled tank stirred by a dual Rushton impeller. For this geometry, LDV measurements show a characteristic dependence of the flow patterns upon the position of the impellers. Two advanced modeling approaches were tested. In the first, the vessel was divided into two concentric blocks, coupled by a sliding grid technique, and simulations were conducted in time-dependent mode. In the second approach, the vessel was modeled as two partially overlapping regions, the inner one rotating with the impeller and the outer one stationary; simulations were run in steady-state mode for each of the two regions, while information was iteratively exchanged between them after azimuthally averaging and transforming for the relative motion. A third set of simulations was conducted for comparison purposes by using a more conventional method, in which the impellers were not explicitly simulated, while their effects were modeled by imposing suitable values of velocities and turbulence quantities (derived from single-impeller experiments) at the blade periphery. The first two techniques gave similar predictions and successfully reproduced the dependence of the flow patterns on the position of the impellers. The latter method required far less computational effort. On the other hand, the impeller boundary conditions technique failed to reproduce the experimental flow patterns, because of the inadequacy of single-impeller boundary conditions for the present geometry.

Introduction

Prediction of flow fields in stirred tanks

The accurate numerical simulation of flow fields in mechanically agitated tanks is highly desirable for a thorough design of equipment and the prediction of important quantities such as power consumption, residence times, and reaction yields (Tatterson, 1994).

In the case of *baffled* tanks, which is by far that most commonly encountered in industrial applications, the simultaneous complete simulation of the (still) baffles and the (rotating) impeller blades requires advanced computational capabilities, such as sliding or deforming grids. Examples of these relatively sophisticated approaches have been presented by Luo et al. (1993, 1994), Issa (1993), Bode (1994), and Tabor et al. (1996) using the STAR-CD code, and by Perng and Murthy (1993), Murthy et al. (1994), and Daskopoulos and Harris (1996) using FLUENT.

A simpler alternative is to exclude the impeller region from the computational domain and substitute for it suitable boundary conditions or suitable sources of momentum and turbulence quantities ("black box" methods). Three-dimensional steady-state predictions based on this approach have been presented, for example, by Middleton et al. (1986), Ranade and Joshi (1989, 1990), Weetman (1991), Gosman et al. (1992), Fokema et al. (1994), and by the present authors (Brucato et al., 1989, 1990). The main limitation of this approach is its lack of generality: experimental data, including turbulence quantities, are needed for each specific case under investigation, but such data are actually available only for a few vessel–impeller geometrical configurations.

Correspondence concerning this article should be addressed to M. Ciofalo.

A computational procedure that, while using standard numerical methods available in most currently available CFD packages, does not require any experimental information was proposed by the present authors (Brucato et al., 1994). This technique, described in detail in the "Impeller Modeling" section of this article, is based on an iterative exchange of information between two concentric but overlapping regions of the vessel, each simulated under *steady-state* assumptions in its own reference frame.

In subsequent work the authors compared the performance of all the cited techniques when applied to the turbulent flow in tanks stirred by *single* radial or axial impellers (Brucato et al., 1998). Predictions were assessed against a variety of quantitative experimental results published in the recent literature. The conclusions were that both the sliding-grid and the authors' "inner–outer" technique were capable of reliably predicting the flow field in stirred vessels—*including* the impeller region—with no recourse to empirical data, thus overcoming the shortcomings of "black box" methods. The two techniques yielded comparable results; the sliding-grid method gave the best agreement with experimental data as regards the mean velocities and presented the advantage of explicitly predicting the time dependence of the flow field, but was more demanding in terms of CPU time and tended to underpredict the kinetic energy of turbulence. The inner–outer method produced the best agreement with experimental data as regards the turbulence quantities, and offered the additional advantage of being viable even with standard computer codes, not explicitly provided with transient sliding/deforming grid capabilities.

In the present work, numerical simulations were conducted for the turbulent flow field in a baffled tank stirred by a *dual* Rushton impeller. For this geometry, recent LDV measurements (Rutherford et al., 1996) show a characteristic dependence of the flow patterns upon the position of the impellers. Therefore, the dual-impeller problem provides an excellent benchmark to assess the *predictive* capability of alternative modeling approaches, such as their ability to correctly reproduce the main qualitative and quantitative features of the flow field without reverting to ad hoc experimental data, specific for the configuration examined. In particular, for the black-box approach mentioned earlier, the crucial point is whether "universal" impeller boundary conditions, derived from experimental measurements in standard tanks, can be applied to configurations characterized by the same impeller, but different overall tank geometries. (In other words: can impeller-dependent, but vessel-independent, peripheral flow fields be used for predictive purposes?)

Clearly, any failure of a modeling technique to reproduce the previously discussed large differences in the flow fields associated with geometry modifications, would shed serious doubts on its suitability for general industrial applications, where detailed experimental data can hardly exist for *all* configurations of interest.

Experimental Results for Dual Rushton Impeller Stirred Tanks

The geometry investigated by Rutherford et al. (1996) is shown in Figure 1, where the relevant nomenclature is also

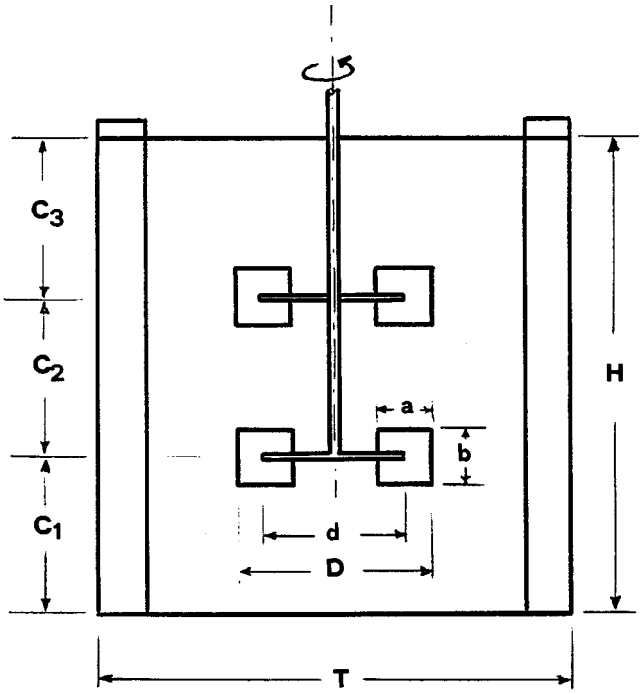

Figure 1. Dual-impeller stirred-reactor configuration.

reported. Measurements were performed for two values of T, 100 mm and 294 mm. In all cases, the liquid height was $H = T$, the width of the four baffles was $b = 0.1\ T$, and the impeller diameter was $D = T/3$. Both impellers were standard Rushton turbines, with the blades aligned in the same vertical planes; the disc and blade thicknesses were 1 mm for the smaller tank and 1.65 mm for the larger. Experiments were conducted at a Reynolds number of 40,000, corresponding to a rotational speed of 2165 rpm (impeller tip speed $V_{tip} = 3.77$ m/s) in the 100-mm vessel and of 250 rpm ($V_{tip} = 1.28$ m/s) in the 294-mm vessel. A lid was used in the smaller vessel, but not in the larger; its presence was assumed to affect the flow field only in the immediate vicinity of the top surface.

A laser-Doppler anemometer, operated in the dual-beam forward-scatter mode with frequency shift, was used to measure all three velocity components in a plane located midway between the two baffles. Both 360-deg-ensemble averaged measurements and 1-deg-resolved measurements were taken. The former yield mean and rms velocity values as seen in the fixed (laboratory) reference frame; the latter yield corresponding values as seen in the rotating reference frame of the impeller. Turbulence energy values derived from the latter measurements do *not* include the low-frequency periodic fluctuations associated with the rotation of the impeller. The power number was also determined by measuring the torque on the shaft with strain gauges.

The experiments showed that the geometrical parameters C_1 (off-bottom clearance of the lower impeller), C_2 (separation between the two impellers), and C_3 (submergence of the upper impeller below the top surface) strongly affect the overall flow structure in the vessel. Only two of these, of course, can be arbitrarily chosen; accordingly, three stable

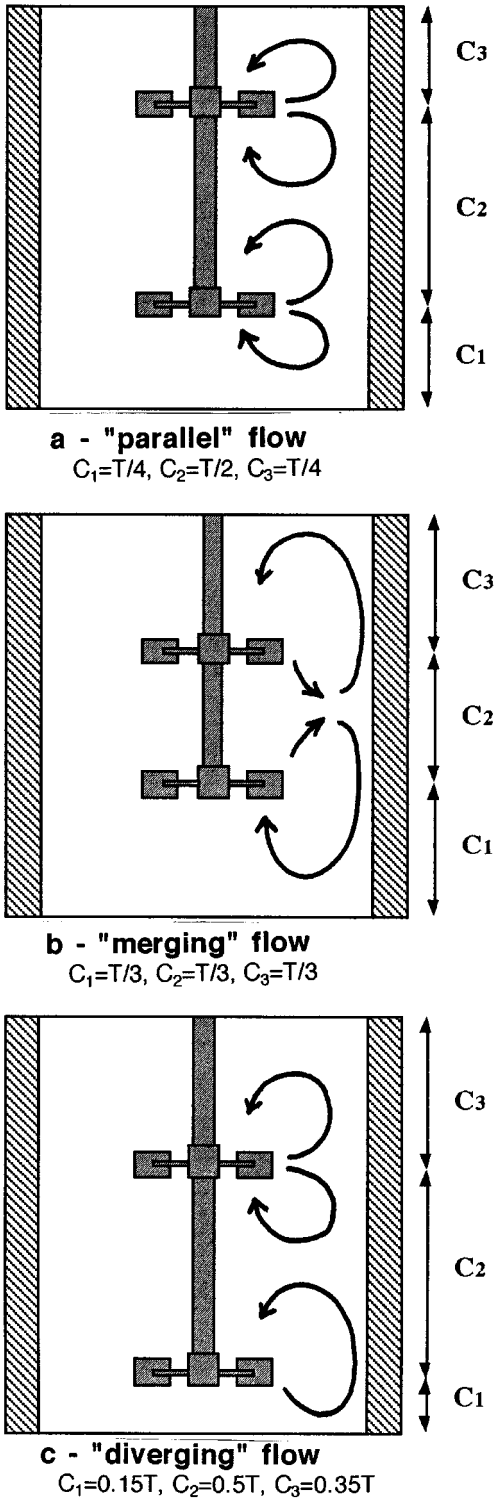

Figure 2. Flow patterns for the three geometrical configurations studied: (a) parallel flow; (b) merging flow; (c) diverging flow.

flow patterns were observed, as qualitatively shown in Figure 2. The *parallel-flow* pattern, with four ring vortices (impellers essentially not interacting), was obtained for $C_1 > 0.20\ T$ and $C_2 > 0.385\ T$. The *merging-flow* pattern, with only two large ring vortices, was obtained for $C_1 > 0.17\ T$ and $C_2 < 0.385\ T$. Finally, the *diverging-flow* pattern was obtained whenever $C_1 < 0.15\ T$ and $C_2 > 0.385\ T$. For intermediate configurations, unstable flow patterns were observed, alternating between any two or all three of the previously cited regimes. Detailed maps of the velocity and turbulence energy distributions are shown in the ''Results'' section of this article, where they will be compared with the authors' predictive results.

Governing Equations, Turbulence Model, and Numerical Methods

With all the impeller modeling approaches compared in this work, the equations to be solved were the Reynolds-averaged continuity and momentum (Navier–Stokes) equations for a constant-density fluid in turbulent motion, written in a cylindrical reference frame of coordinates r, θ, z. Turbulence was modeled by using the standard k-ϵ model with ''wall functions'' on solid walls (Launder and Spalding, 1974). With the computational grids used (see below), the dimensionless distance from the wall was of the order of 10^2 for most of the near-wall grid points (control volume centers). The unknowns of the problem were the pressure p, the three velocity components u_r, u_θ, and u_z, the turbulence energy k, and its dissipation rate ϵ. Details are quite standard and therefore will not be given here; they can be found, for example, in Ciofalo et al. (1996).

The equations were written in their time-dependent form only when the ''sliding-grid'' approach was adopted, while steady-state conditions were assumed with the other two techniques. Appropriate centrifugal and Coriolis body forces were included for the ''inner'' simulations, which were conducted in the rotating reference frame of the impeller.

The numerical solution of the governing equations was achieved by a finite-volume method (Burns and Wilkes, 1987), implemented in the computer code CFDS-FLOW3D (AEA Technology, 1994). It is based on a colocated grid approach and relies on the Rhie–Chow (1983) algorithm to prevent ''chequerboard'' oscillations. The SIMPLEC algorithm (VanDoormal and Raithby, 1984) was used to couple the continuity and Navier–Stokes equations, and the hybrid-upwind discretization scheme was used for the convective terms.

Impeller Modeling

As mentioned earlier, three different approaches to the modeling of the impeller were used in this work. They are analyzed in further detail below.

Impeller boundary-condition method

In the traditional impeller boundary condition (IBC) approach steady-state conditions are imposed and simulations are conducted in the laboratory reference frame. Therefore, transient terms and body forces disappear from the transport equations. Azimuthally uniform values of u_r, u_θ, u_z, k, and ϵ, functions of z only, are imposed in the cells belonging to the vertical cylindrical layer bounding the impeller-swept volumes. From the numerical point of view, this is accomplished by appropriately modifying the coefficients and righthand

Table 1. Values Adopted for the Impeller Boundary Conditions

z/b*	u_r/V_{tip}	u_θ/V_{tip}	u_z/V_{tip}	k/V_{tip}^2	$\epsilon/\langle\epsilon\rangle$**
0.44	0.122	0.165	0	0.061	10.5
0.33	0.195	0.237	0	0.087	15.0
0.22	0.392	0.467	0	0.108	13.4
0.11	0.620	0.610	0	0.114	7.3
0	0.740	0.670	0	0.120	5.0
−0.11	0.620	0.610	0	0.114	7.3
−0.22	0.392	0.467	0	0.108	13.4
−0.33	0.195	0.237	0	0.087	15.0
−0.44	0.122	0.165	0	0.061	10.5

*Coordinate z centered at the impeller's midplane.
**$\langle\epsilon\rangle$ = average dissipation rate in the vessel, based on a power number $N_p = 5$.

sides of the corresponding linearized transport equations at each SIMPLEC iteration.

The flow field in the impeller region is computed as in any other part of the computational domain. The impellers' shaft, hub, and disc, although not its blades, are explicitly described as solid volumes. In order for periodicity conditions to be applied along θ, the azimuthal extent of the computational domain must include at least one baffle, independent of the number of impeller blades, and was therefore $\pi/2$ in the present case.

The numerical values of the imposed quantities were based on the experimental LDV results of Wu and Patterson (1989) and are reported in Table 1. They were obtained in a baffled tank stirred by a single Rushton turbine having $D/T = 1/3$ and located at a distance $T/3$ from the vessel bottom. The Reynolds number was about 10^5. Only the ''truly'' turbulent components of k and ϵ, not inclusive of the low-frequency components associated with the periodic passage of the blades, were considered.

Clearly, the preceding configuration is quite different from the dual-impeller geometry of the problem studied here. As discussed previously, the adoption of these ''improper'' impeller boundary conditions is not only a forced choice, due to the lack of detailed experimental data at the impellers' periphery for the current dual-impeller configuration, but also a way of checking the predictive value of the IBC method for problems in which the overall tank geometry differs from the experimental one.

Sliding-grid method

The sliding-grid (SG) approach makes use of the multiblock and transient grid capabilities of CFDS-FLOW3D (Releases 3.3 and following). The flow domain is divided into two cylindrical, nonoverlapping subdomains, each gridded as a separate block: the outer one is fixed in the laboratory reference frame, while the inner one rotates along with the impellers. Unlike the inner–outer method described below and in the Multiple Frame of Reference (MFR) method of Luo et al. (1993, 1994), the flow equations in the inner subdomain are formally written with respect to the *laboratory* reference frame, while it is the grid that rotates. However, grid rotation results in acceleration terms that are completely equivalent to the apparent body forces arising in noninertial frames.

The two regions are implicitly coupled at the interface separating the two blocks via a sliding-grid algorithm, which takes into account the relative motion between the two subdomains and performs the necessary interpolations.

Simulations are conducted in transient mode, and the computation is stopped when a satisfactory time periodicity has been attained. In order for periodicity boundary conditions to be imposed in the azimuthal direction, the computational domain must include an integral number, both of blades and of baffles; thus, its computational extent was 180 deg in the present case (six blades, four baffles).

The results of a ''sliding grid'' simulation are space- and time-dependent fields of the mean flow and of turbulence quantities. In order to make comparisons with ensemble-averaged LDV data and with IBC/IO predictions consistent, results were averaged here over a complete revolution of the impeller, thus making them independent of the position relative to the blades.

Inner–outer iterative procedure

In the inner–outer (IO) iterative approach, the vessel is subdivided into two partially overlapping zones, as shown in Figure 3: an inner domain containing the impeller, and an outer one including the baffles. The computation proceeds through the following steps:

1. First, a simulation of the flow in the inner domain is carried out in a reference frame rotating with the impeller, with arbitrary boundary conditions (e.g., still fluid) imposed on the surface Σ_e (Figure 3a). Since the reference frame is a noninertial one, centrifugal and Coriolis forces have to be included in the momentum equations. A first trial flow field is thus computed in the whole impeller region, including the distributions of velocity, turbulence energy, and dissipation on the boundary surface Σ_i.

2. The latter distributions on Σ_i are now used as boundary conditions for a first simulation of the flow in the outer domain (Figure 3b); this is carried out exactly as in the IBC method, in the inertial reference frame of the laboratory. Information on the flow field in the whole vessel is thus obtained, including, in particular, a first estimate of velocity, turbulent kinetic energy, and dissipation on the boundary surface Σ_e.

3. The latter values are now used as boundary conditions for a second inner simulation, and so on, until the system attains a satisfactory numerical convergence.

Each of the inner and outer simulations is conducted under steady-state assumptions in its own reference frame. Since the two frames are different, the information that is iteratively exchanged (velocity, turbulence energy, and dissipation on the boundary surfaces Σ_i and Σ_e) is *corrected for the relative motion* and is *averaged over the azimuthal direction.*

A crucial feature of this approach is the existence of an *overlap* region, common to the inner and outer domains, which provides the iterative matching of the two solutions; the extent of this region, and the exact location of its boundaries, are largely immaterial. By contrast, in the MFR method of Luo et al. (1993, 1994), the inner and outer steady-state solutions are implicitly matched along a single boundary surface, and external iterations are not required. On the other hand, the choice of this surface is *not* arbitrary, since it has

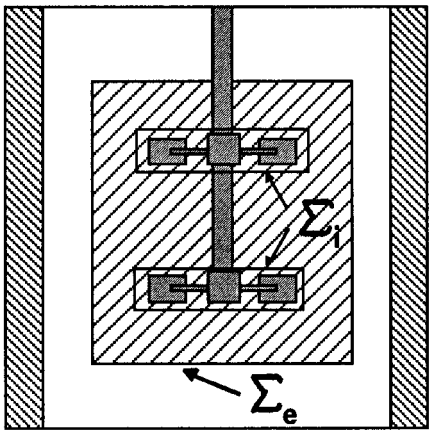

(a)

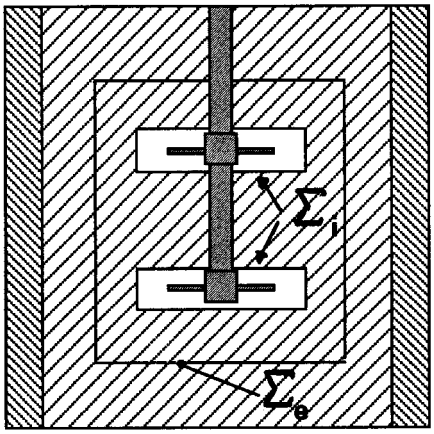

(b)

Figure 3. Inner–outer procedure: the shaded regions are the computational domains for the " inner" (a) and the " outer" (b) simulations.

Σ_i, Σ_e: surfaces on which boundary conditions are iteratively imposed.

to be assumed *a priori* as a surface where flow variables do not change appreciably either with θ or with time (although a "predictor-corrector" approach can be used in order to locate the stationary interface more exactly).

It should be observed that the azimuthal extents of the two inner and outer computational domains need not be the same; in particular, for periodicity conditions to be applied along the azimuthal direction, it is sufficient that the inner domain include just one blade and the outer domain just one baffle.

Note that the low-frequency periodic velocity variation (associated with the passage of the blades), which would be observed at a point on Σ_i in the reference frame of the laboratory, is equivalent to the azimuthal velocity variation computed along Σ_i in the inner simulation. Conversely, the low-frequency periodic velocity variation (associated with the passage in front of the baffles), which would be observed at a point on Σ_e in the reference frame of the impeller, is equivalent to the azimuthal velocity variation computed along Σ_e in the outer simulation. One-half of the corresponding variance may or may not be included in the boundary conditions for the turbulence energy k when the inner and outer solutions are iteratively matched. As discussed below, results are only marginally affected by this choice.

Test cases, grids, and computational aspects

The test cases that were numerically simulated are summarized in Table 2. They correspond to the parallel flow, merging flow, and diverging flow regimes, respectively, as experimentally observed by Rutherford et al. (1996). For each of the three test geometries simulated, the same basic mesh-point distribution was adopted with all the impeller modeling approaches used. For case A ($C_1 = C_3 = 0.25\ T$, $C_2 = 0.5\ T$), the computational domain and the grid are shown in Figure 4. Their azimuthal extent of $\pi/2$ applies to the simulations conducted using the IBC approach as well as to the outer part of the simulations conducted by the IO approach. The inner simulations of the latter were limited to an azimuthal extent of $\pi/3$ (spacing between two consecutive impeller blades) and to a computational domain that also was reduced in the radial and axial directions, as shown in Figure 3a. On the other hand, sliding-grid simulations were conducted on a computational domain whose azimuthal extent was π (twice that in Figure 4) for the periodicity reasons discussed earlier.

The grid in Figure 4 included 86 cells along the axis, 42 along the radius, and 18 along the azimuthal direction, covering an angle of $\pi/2$. Each impeller blade was resolved by 9 axial and 10 radial cells. Preliminary tests confirmed that this resolution was amply sufficient to guarantee that results were essentially grid-independent.

All simulations were run on an HP-712 RISC workstation with 64 Mbytes RAM. Typical computing times were about 60 s/iteration for steady-state simulations (IBC and IO techniques). Thus, IBC simulations, which were protracted for 3000 iterations, required about 50 h of computing time, while IO simulations, involving 4000 outer and 4000 inner overall iterations, required about 100 h of computing time.

With the SG time-dependent approach, preliminary simulations suggested that, at least for the merging and diverging flow configurations, a satisfactory time-periodicity could be attained only after a very large number of revolutions of the impellers (more than 20). This result is consistent with experimental observations by Yianneskis and coworkers (private communication). They reported that, following the impellers' startup, a roughly parallel flow pattern was initially observed independent of the impeller configuration; this then developed slowly and eventually attained its final merging or diverging shape only after 20 to 30 impeller revolutions.

Table 2. Test Cases Simulated

Case	C_1	C_2	C_3	Notes
A	0.25 T	0.50 T	0.25 T	Parallel flow
B	0.33 T	0.33 T	0.33 T	Merging flow
C	0.15 T	0.50 T	0.35 T	Diverging flow

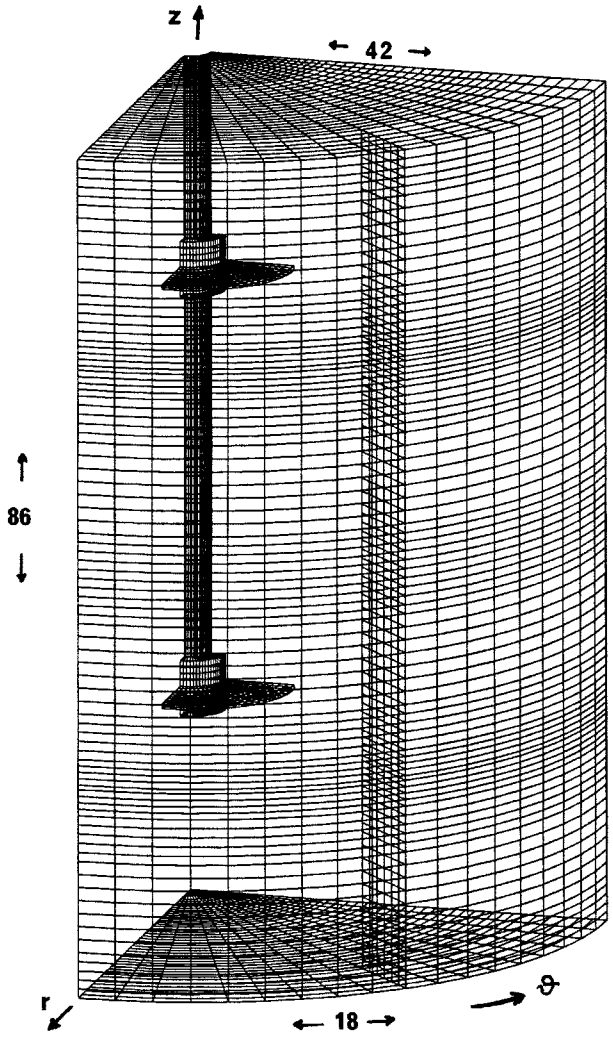

Figure 4. Computational grid used for the " outer" simulations in the IO procedure (test case A); the number of grid cells along each direction is reported.

An accurately time-resolved simulation of such a long transient was prohibitive in terms of computing time, and unnecessary as far as only the final, time periodic state was the purpose of the computation. Therefore, the following compromise strategy was adopted: the overall simulation was protracted for 60 impeller revolutions, largely sufficient for time-periodic conditions to be attained, but the first 55 revolutions were simulated using a very coarse time step ($\Delta t = 1$ revolution period), while only the final 5 revolutions were simulated by a much finer step ($\Delta t = 1/72$nd of a revolution period), so that the grid rotated by exactly one azimuthal cell at each step.

Even so, SG simulations were highly computationally demanding. More precisely, 55 time steps were required for the startup phase and 360 for the final refinement phase; the number of SIMPLEC iterations per time step was chosen to be 15 for the former and 25 for the latter, so that, on the whole, 9,825 iterations were conducted for each test case. Due to the larger computational domain, the grid included twice as many cells ($\sim$140,000) than with the other two methods, so that the CPU time per iteration was correspondingly larger ($\sim$120 deg). Therefore, a single simulation required about 320 h of CPU time. Moreover, the grid was too large for completely in-core calculations, so that frequent disk access was necessary and the total throughput time was about twice as large as the CPU time (thus amounting to almost one month for each simulation!).

Results and Discussion

For case A (parallel flow), a comparison of predictions obtained by different impeller modeling techniques with experimental LDV data is reported in Figures 5 to 8. All graphs are for a plane at 45 deg between two consecutive baffles; graphs relative to the inner–outer technique report predictions obtained in the outer computational domain.

Figure 5 reports vector plots of the in-plane velocity field. All models correctly predict the overall flow pattern in the stirred tank, including the location of the recirculation centers and the rate of spreading of the radial jet issuing from the impeller. The differences between the three approaches are only marginal and regard mainly the near-impeller flow, with the SG technique yielding the sharpest curvature of the streamlines.

Figure 6 reports axial profiles of the radial velocity u_r (normalized by V_{tip}) at different radial locations: $r = 0.18\ T$ (immediately outside of the blade edges); $0.25\ T$; and $0.39\ T$ (close to the radial location of the baffle edges). Only IO and SG (i.e., fully predictive) results were included; experimental profiles were obtained from the published vector plots of Rutherford et al. (1996), and thus are to be taken with some caution. Nevertheless, these graphs allow a more quantitative assessment of the predictions than the vector plots given previously. Some underprediction of peak velocities by both computational methods can be observed at $r = 0.18\ T$ and $0.25\ T$, graphs (a) and (b), while a better agreement is obtained at some distance from the impeller, graph (c). IO and SG predictions differ only marginally.

Contour plots of the turbulence energy k (normalized by V_{tip}^2) are compared in Figure 7. In order to make a quantitative assessment easier, axial profiles of k also are shown for two radial locations ($0.18\ T$ and $0.25\ T$) in Figure 8, which includes only predictions obtained by the IO and SG techniques. As for the mean velocity results in Figures 5 and 6, experimental data were read from the published figures and thus are to be taken with some caution; in particular, no contour could be reported for levels of k below $0.027\ V_{tip}^2$, that is, in low-turbulence regions. Levels of turbulence energy are underpredicted by all computational methods. The lowest values of k are given by the IBC technique, Figure 7b, while the IO and SG predictions are almost identical and in better agreement with the experimental results (see Figures 7c and 7d or Figure 8). Some underprediction of the turbulence energy is a common feature of stirred-tank simulations (see Daskopoulos and Harris, 1996), and appears to be an inherent shortcoming of the k-ϵ model for such flows.

Predictions of the mean velocity and turbulence field for case B (merging flow) are compared with experimental re-

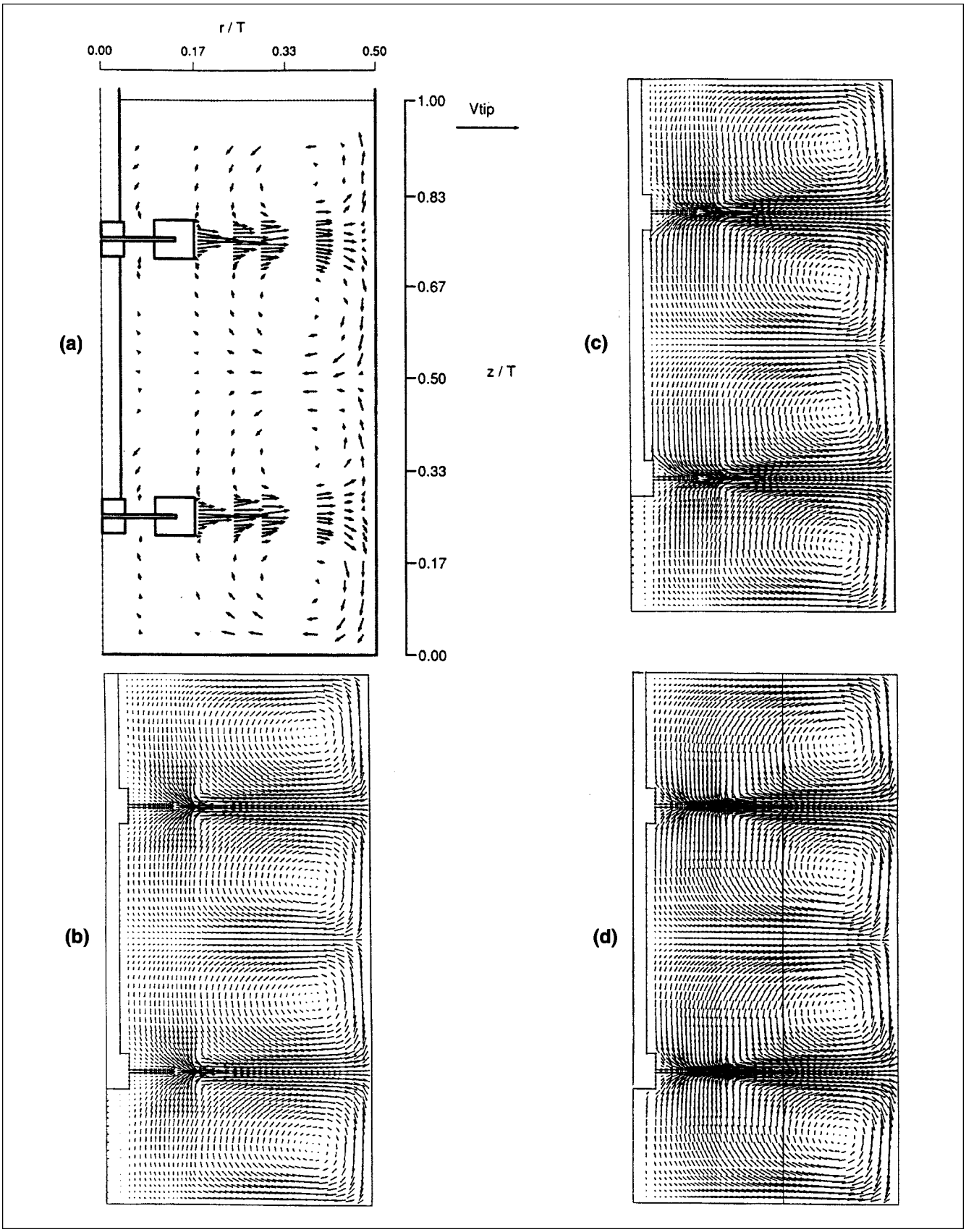

Figure 5. Parallel flow: comparison of velocity vector plots in a plane midway between baffles.

(a) Experimental results (Rutherford et al., 1996); (b) predictions, IBC technique; (c) predictions, IO technique; (d) predictions, SG technique.

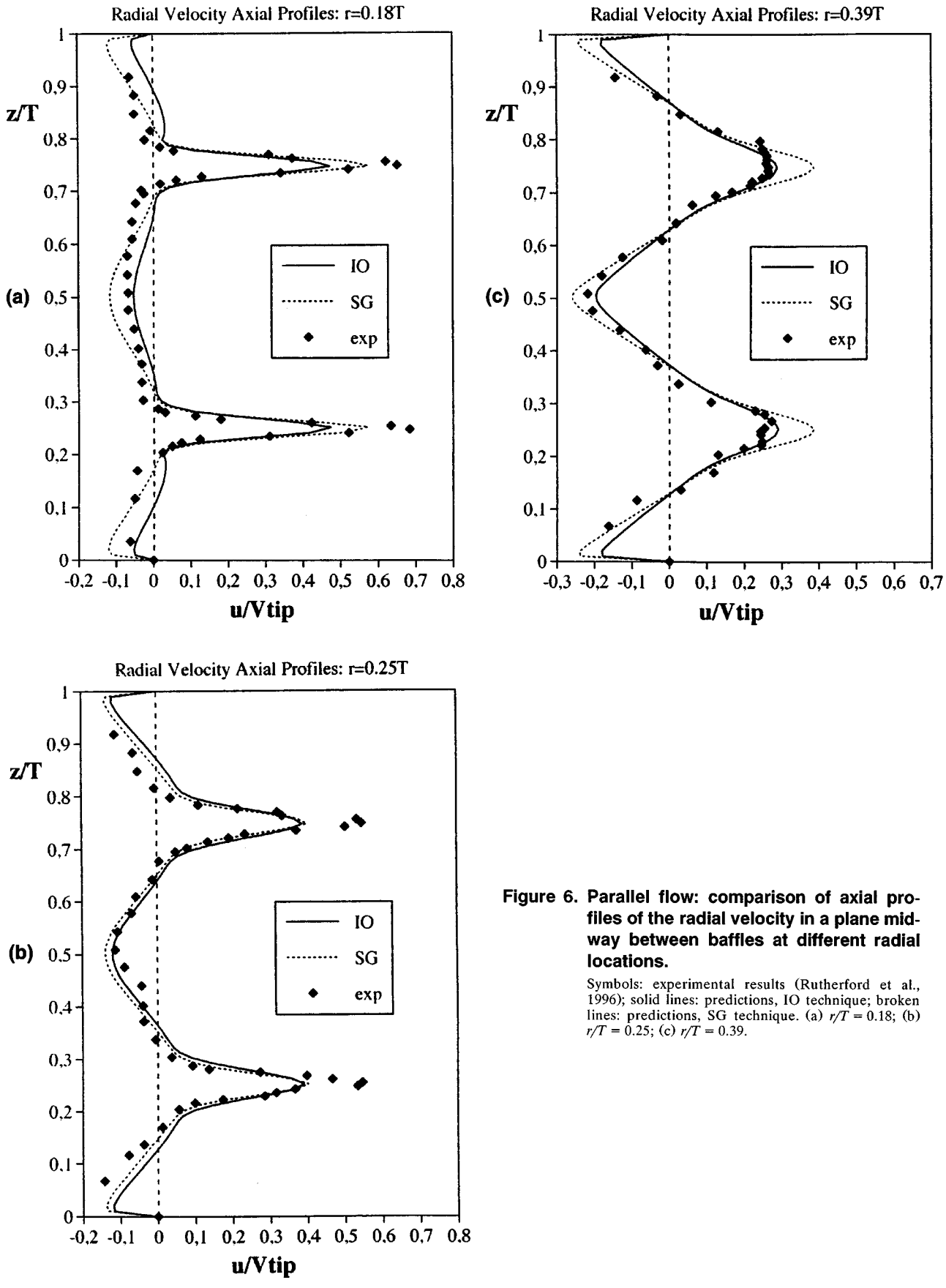

Figure 6. Parallel flow: comparison of axial profiles of the radial velocity in a plane midway between baffles at different radial locations.

Symbols: experimental results (Rutherford et al., 1996); solid lines: predictions, IO technique; broken lines: predictions, SG technique. (a) $r/T = 0.18$; (b) $r/T = 0.25$; (c) $r/T = 0.39$.

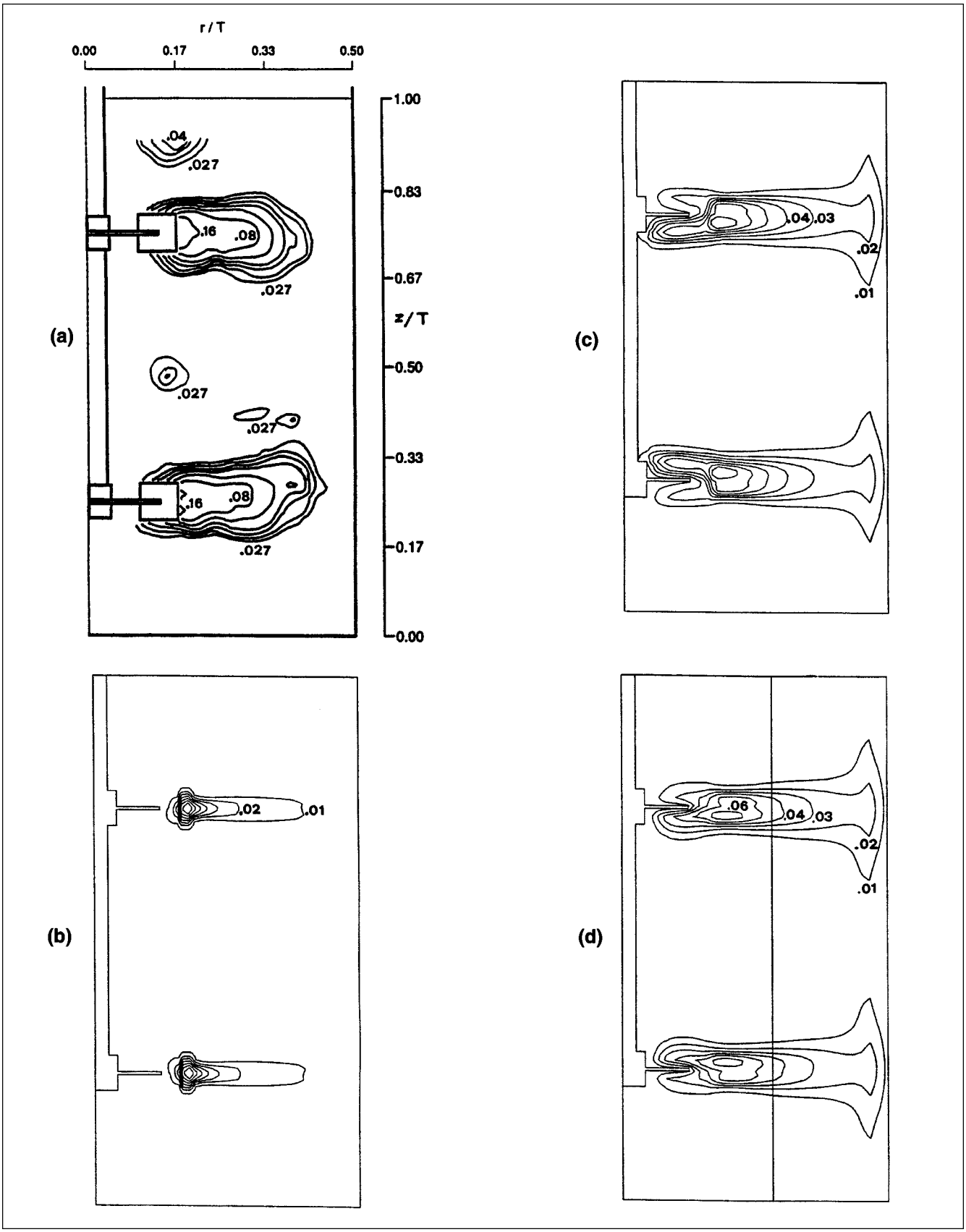

Figure 7. Parallel flow: comparison of turbulence energy distributions in a plane midway between baffles.

(a) Experimental results (Rutherford et al., 1996); (b) predictions, IBC technique; (c) predictions, IO technique; (d) predictions, SG technique.

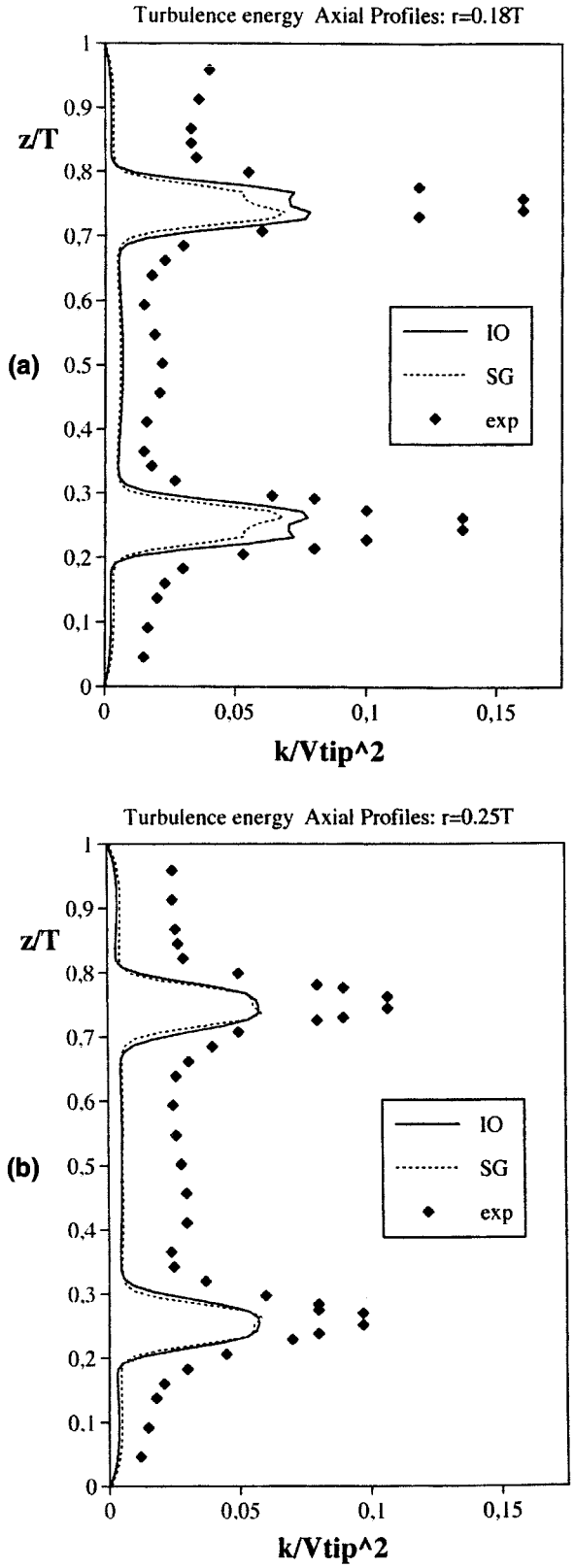

Figure 8. Parallel flow: comparison of axial profiles of the turbulence energy in a plane midway between baffles at different radial locations.

Symbols: experimental results (Rutherford et al., 1996); solid lines: predictions, IO technique; broken lines: predictions, SG technique. (a) $r/T = 0.18$; (b) $r/T = 0.25$.

sults in Figures 9 to 12. These are organized the same as Figures 5–8, relative to the parallel flow case.

The vector plots in Figure 9 show clearly that only the SG and IO techniques successfully reproduce the characteristic merging flow pattern that is experimentally observed for this configuration, while the IBC method yields a four-loop velocity field that is qualitatively similar to that predicted for the parallel-flow configuration. The experimental velocity vectors show that the distortion of the radial jets issuing from the impellers, due to the attractive interaction between the two streams (a phenomenon akin to the Coanda effect observed in near-wall planar jets), extends upstream to the impeller periphery (and probably to the flow between the impeller blades itself). Therefore, the failure of the IBC method, which is based on undistorted experimental velocity profiles at the impeller boundary, to predict the overall flow fields is not surprising: apparently, imposing a horizontal outflow at the impeller periphery forces the overall flow field toward the ''double eight'' configuration characteristic of the parallel-flow regime. This result simply confirms that universal impeller outflow profiles do *not* exist, and that the IBC technique can be reliably applied only if experimental data for the flow at the impeller's periphery are available for the *overall* (impeller + vessel) configuration under study (or at least for closely similar geometries), which seriously impairs the predictive power of the method.

A close examination of the vector plots in Figure 9 reveals that both the IO and the SG methods actually *overpredict* the convergence of the two impeller streams. The angle formed by these with the horizontal was about 35 deg in the experiments, graph (a), while it is ~ 45 deg in the IO predictions, graph (c), and even higher in SG predictions, graph (d).

This shortcoming of the computational results is better evidenced by the axial profiles of u_r reported in Figure 10. As a consequence of the excessive convergence of the two impeller streams, the radial velocity is severely underpredicted close to the impeller periphery ($r = 0.18\ T$, graph 10a) and also at the intermediate location $r = 0.25\ T$ (graph 10b), where the experimental data show two still separate streams and a central reverse flow region, while the simulations yield outflow even in the vessel midplane. Note that, due to the smaller convergence angle, IO predictions behave slightly better, showing at least two separate maxima for u_r. A satisfactory agreement with the experimental data is obtained only at a larger distance from the impeller ($r/T = 0.39$, graph 10c), where the two streams also have completely merged also in the experiments.

Turbulence energy contour plots are shown in Figure 11. IBC predictions were not included here, since the inability of the IBC technique to correctly reproduce the flow patterns in these cases would make a comparison of the corresponding k distributions meaningless. Levels of k are underpredicted by both the IO and SG methods, while the shape of the contours reflects the behavior of the impeller streams as regards their angle with respect to the horizontal. The experimental data (graph 11a) show that k decreases along the two streams as one moves from the impellers to the midplane; this trend is still recognizable, but greatly attenuated, in the IO results (graph 11b), and is completely absent in the SG predictions (graph 11c), which exhibit a maximum of k in the midplane.

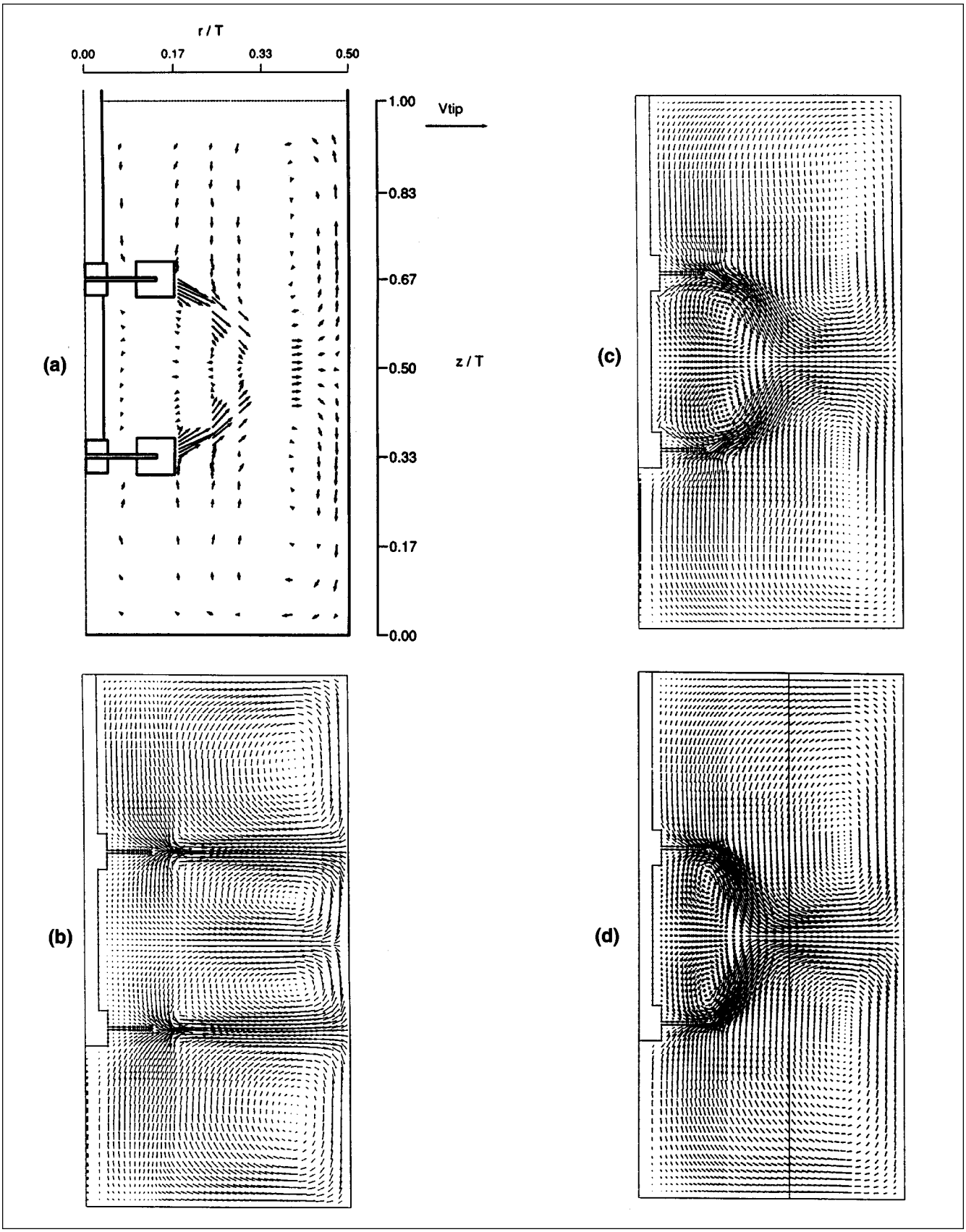

Figure 9. Merging flow: comparison of velocity vector plots in a plane midway between baffles.

(a) Experimental results (Rutherford et al., 1996); (b) predictions, IBC technique; (c) predictions, IO technique; (d) predictions, SG technique.

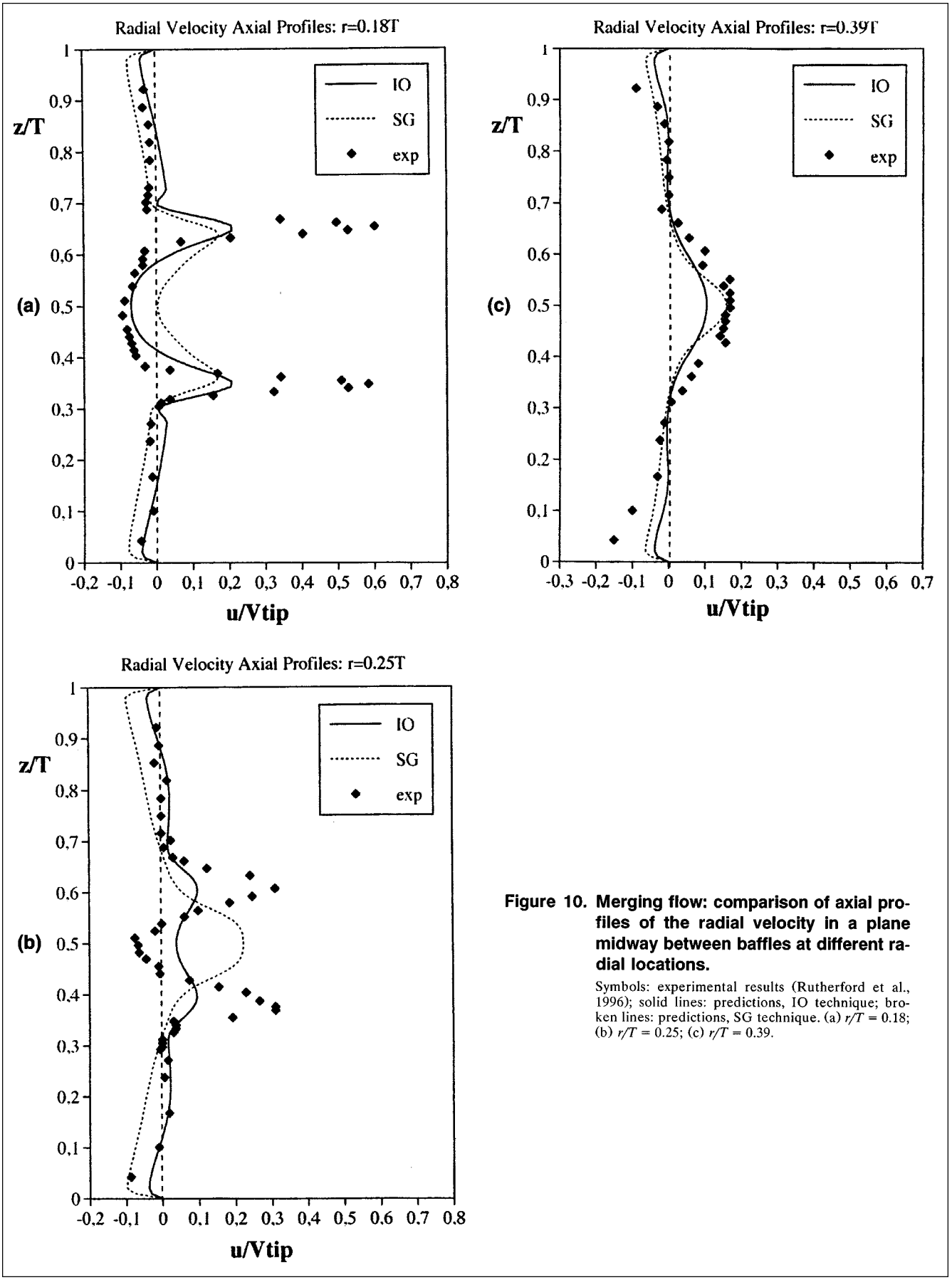

Figure 10. Merging flow: comparison of axial profiles of the radial velocity in a plane midway between baffles at different radial locations.

Symbols: experimental results (Rutherford et al., 1996); solid lines: predictions, IO technique; broken lines: predictions, SG technique. (a) $r/T = 0.18$; (b) $r/T = 0.25$; (c) $r/T = 0.39$.

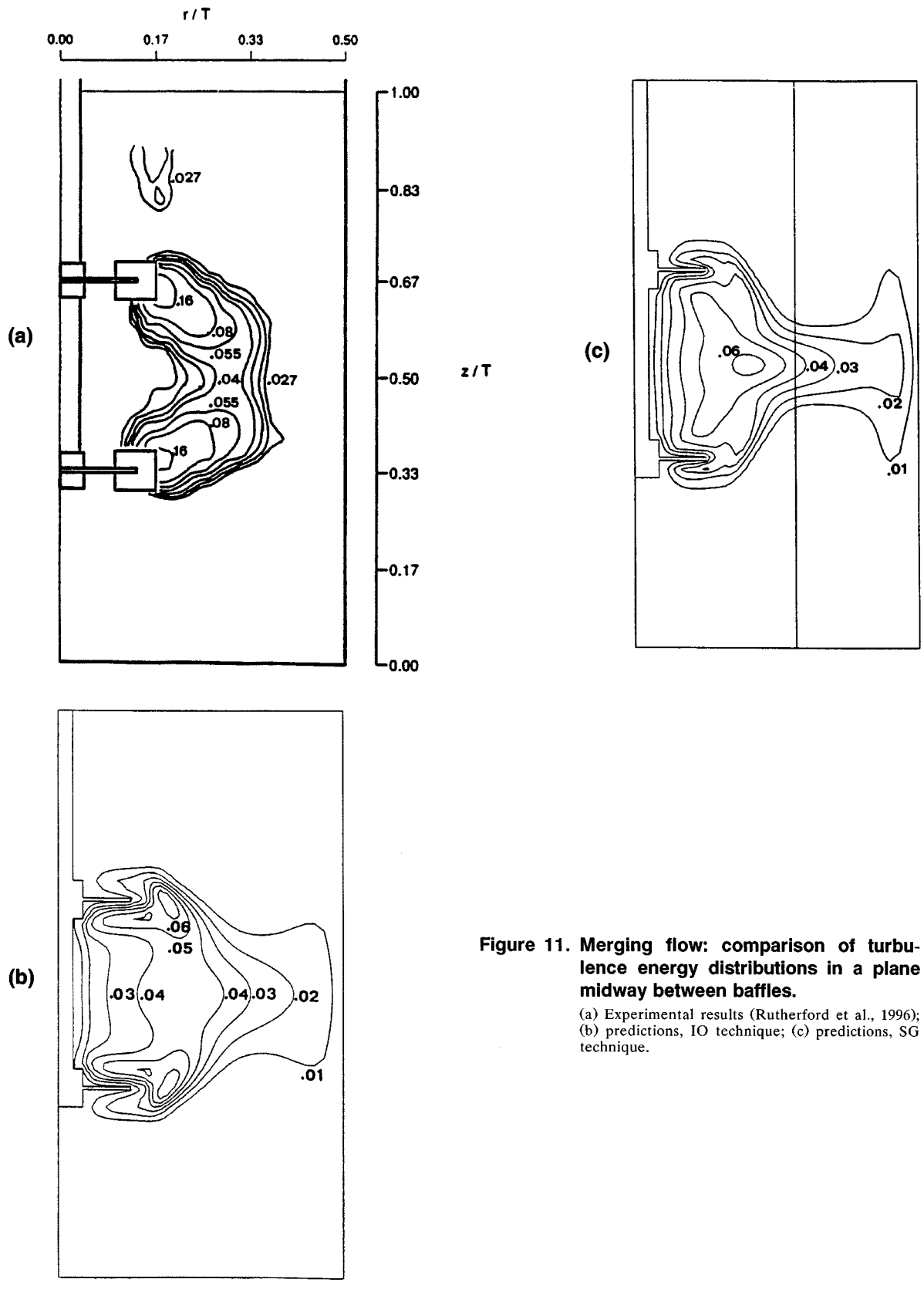

Figure 11. Merging flow: comparison of turbulence energy distributions in a plane midway between baffles.

(a) Experimental results (Rutherford et al., 1996); (b) predictions, IO technique; (c) predictions, SG technique.

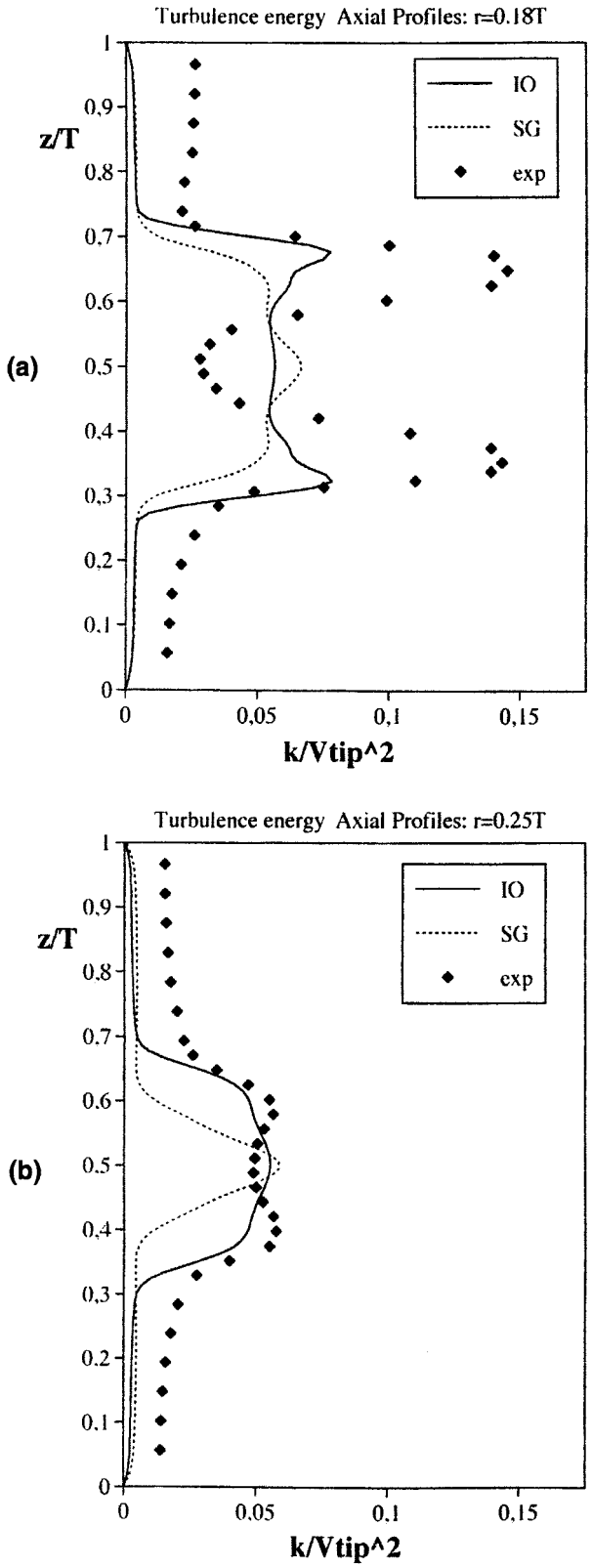

Figure 12. Merging flow: comparison of axial profiles of the turbulence energy in a plane midway between baffles at different radial locations.

Symbols: experimental results (Rutherford et al., 1996); solid lines: predictions, IO technique; broken lines: predictions, SG technique. (a) $r/T = 0.18$; (b) $r/T = 0.25$.

The preceding remarks are confirmed by the axial profiles of k reported in Figure 12. Close to the impeller periphery ($r = 0.18\ T$, graph 12a), IO profiles underpredict k by about double, but still exhibit a double-peak shape, while SG results show a maximum of k in the vessel midplane. Levels of k are satisfactorily reproduced by IO predictions farther from the impeller ($r = 0.25\ T$, graph 12b), while SG results are significantly lower along most of the vessel height.

The significant overprediction of k in the space between the impellers, together with its underprediction along the axis of the streams, suggest that the lateral diffusion of turbulence energy is being overpredicted. In turn, high levels of k near the midplane result in high dissipation rates and in the establishment of a low-pressure region that attracts the impeller streams, leading to the observed overprediction of their convergence angle. This behavior is probably an inevitable shortcoming of the k-ϵ turbulence model and seems to be related with its commonly reported underprediction of reattachment lengths in separated flows.

Finally, results for case C (diverging flow), arranged as for the previous geometries, are reported in Figures 13 to 16.

The vector plots in Figure 13 show that also for this configuration the IBC method fails completely to predict the overall flow pattern, yielding parallel streams. Both the SG and IO methods correctly reproduce the characteristic attachment of the lower stream to the bottom wall, but overpredict its downward curvature (the angle with respect to the horizontal was about 30 deg in the experiments, while IO/SG results exhibit a 45–50-deg value).

Axial profiles of the radial velocity confirm this behavior, showing a severe underprediction of u_r in the lower stream close to the impeller periphery ($r = 0.18\ T$, graph 14a). Levels of u_r are fairly well reproduced farther away from the impeller ($r = 0.25\ T$ and $0.39\ T$, graphs 14b and 14c), although the location of the peak is much closer to the bottom wall than the experimental data indicate. SG predictions are slightly higher and closer to the experimental values than IO predictions. In the upper impeller, both experimental and numerical results are very close to those obtained for the parallel flow configuration, Figure 6, showing that the two impellers do not interact.

Contour plots of the turbulence energy k are reported in Figure 15. As in the merging-flow case, IBC predictions were not included. The same remarks as before hold as regards the accuracy of the reported experimental data. The overall agreement of SG and IO predictions with the experimental results is of the same order as that observed for the merging flow case (Figure 11). Of course, the shape of the k contours reflects the behavior of the impeller stream, with the just discussed overprediction of the inclination angle. Moreover, the rapid dissipation of k near the walls indicated by the experimental data seems to be somewhat underpredicted by the numerical simulations.

The axial profiles of k reported in Figure 16 confirm that the underprediction of turbulence energy is comparable to that observed in the merging flow configuration. IO results are consistently higher than SG predictions, a trend opposite to that observed for the radial velocity in Figure 14.

The (negligible) influence of the low-frequency, periodic velocity fluctuations associated with the rotation of the impeller in numerical IO or SG simulations is illustrated in Fig-

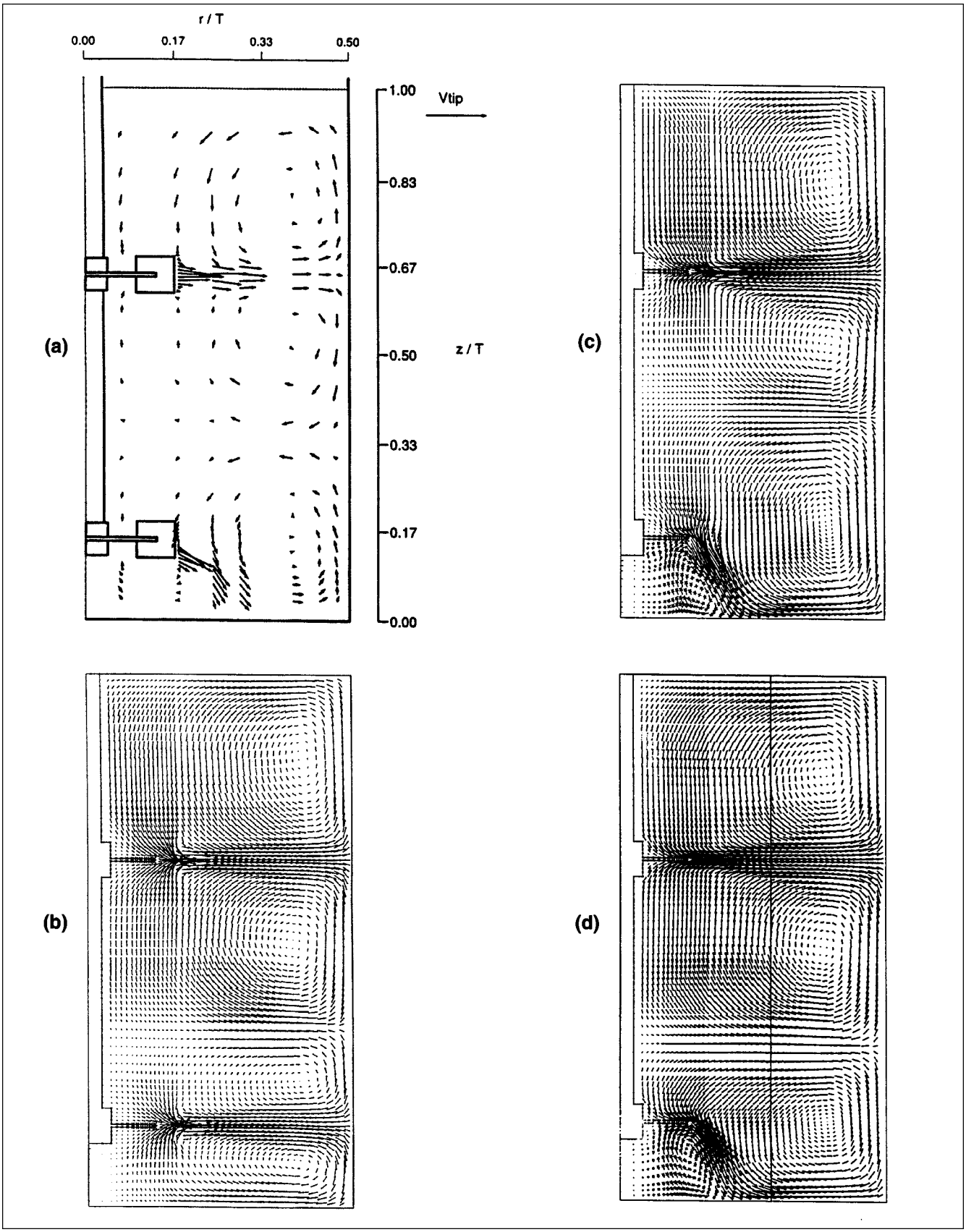

Figure 13. Diverging flow: comparison of velocity vector plots in a plane midway between baffles.

(a) Experimental results (Rutherford et al., 1996); (b) predictions, IBC technique; (c) predictions, IO technique; (d) predictions, SG technique.

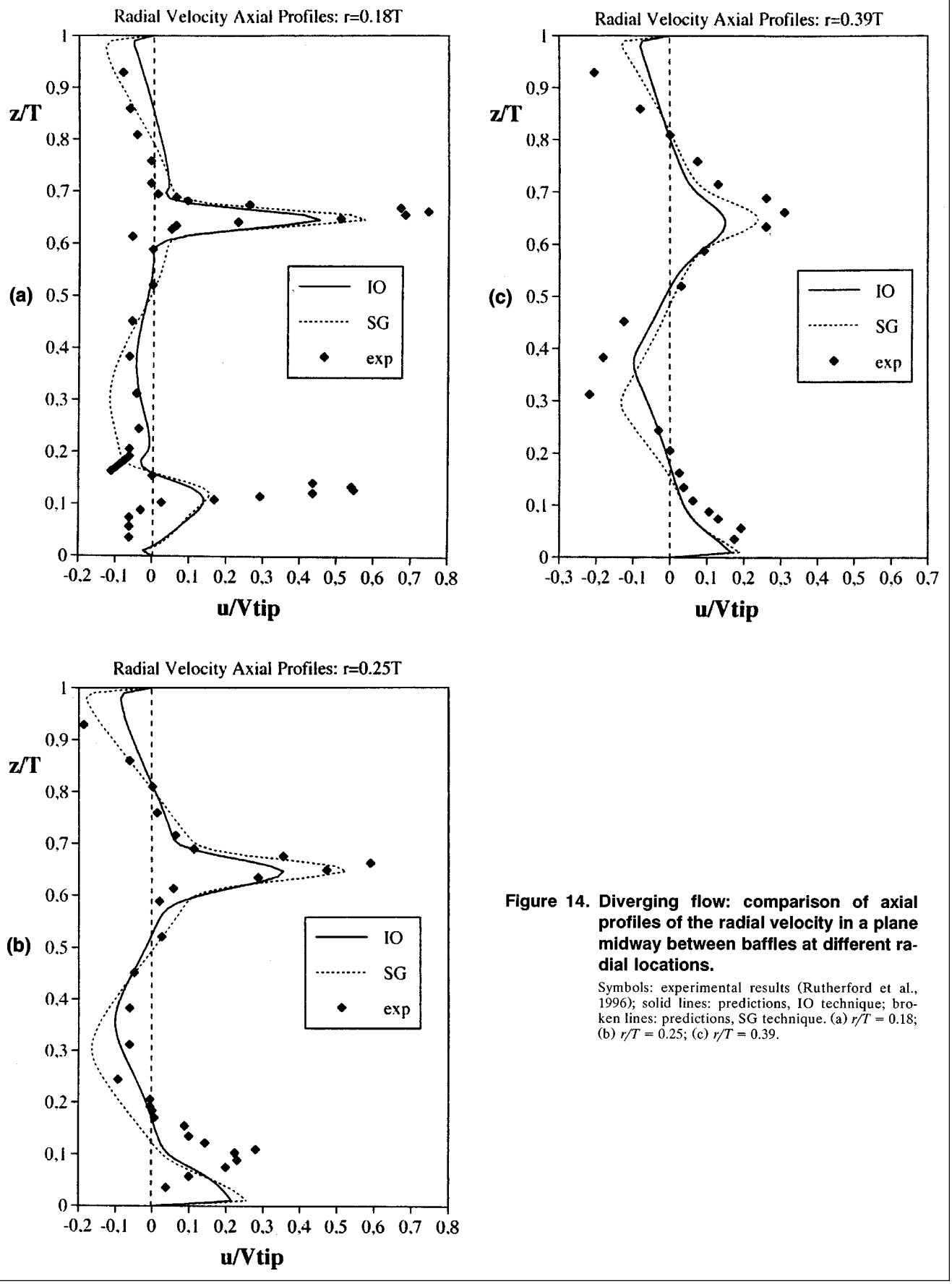

Figure 14. Diverging flow: comparison of axial profiles of the radial velocity in a plane midway between baffles at different radial locations.

Symbols: experimental results (Rutherford et al., 1996); solid lines: predictions, IO technique; broken lines: predictions, SG technique. (a) $r/T = 0.18$; (b) $r/T = 0.25$; (c) $r/T = 0.39$.

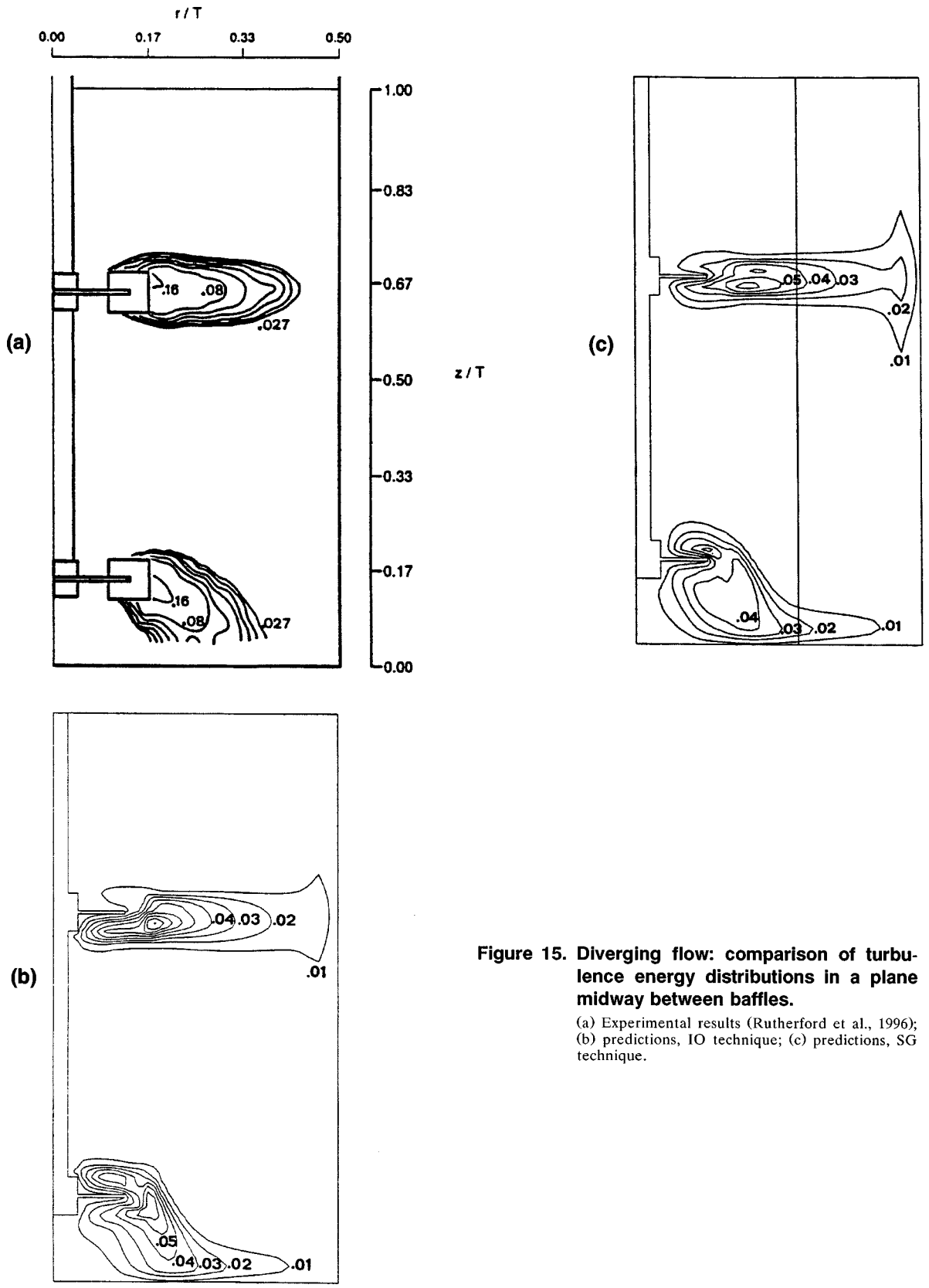

Figure 15. Diverging flow: comparison of turbulence energy distributions in a plane midway between baffles.

(a) Experimental results (Rutherford et al., 1996); (b) predictions, IO technique; (c) predictions, SG technique.

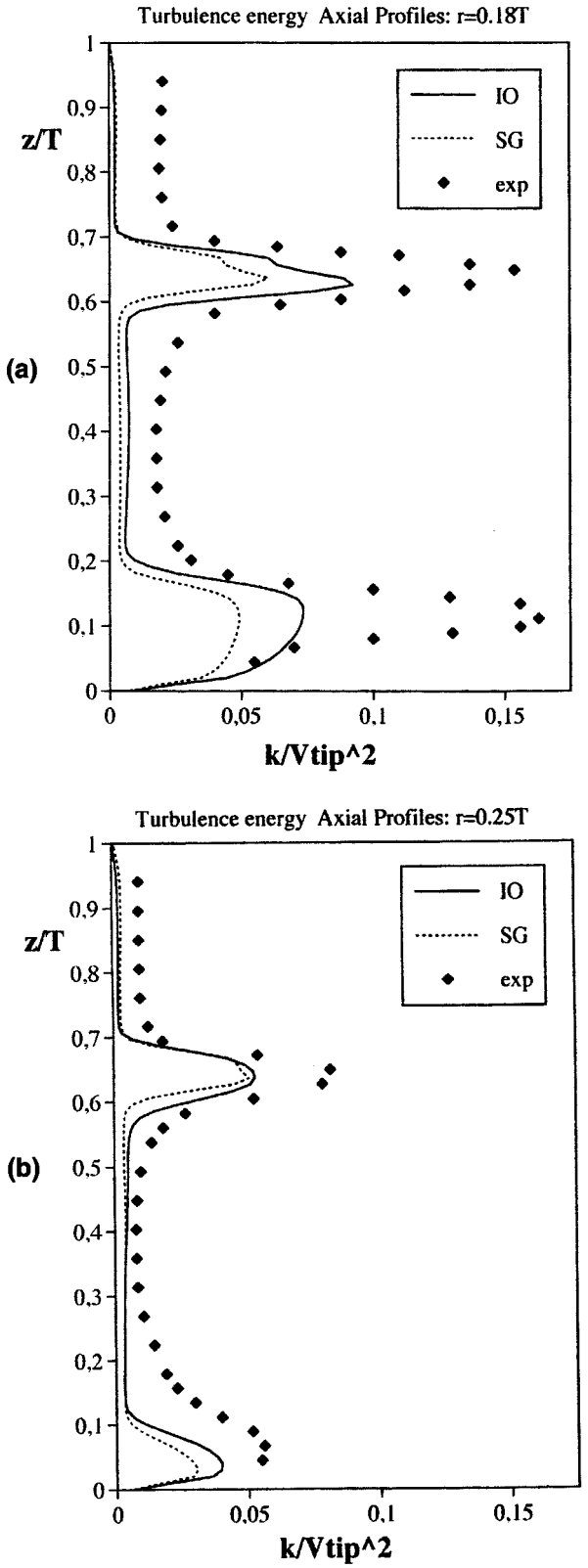

Figure 16. Diverging flow: comparison of axial profiles of the turbulence energy in a plane midway between baffles at different radial locations.

Symbols: experimental results (Rutherford et al., 1996); solid lines: predictions, IO technique; broken lines: predictions, SG technique. (a) $r/T = 0.18$; (b) $r/T = 0.25$.

ure 17. As mentioned in an earlier section, in IO simulations these low-frequency terms appear as azimuthal velocity variations along the surfaces Σ_i and Σ_e and may or may not be included in the boundary conditions for the turbulence energy k when the inner and outer solutions are iteratively matched. All the results discussed so far were obtained *without* such terms; Figure 17a reports the turbulence energy distributions computed for the case of diverging flow in a plane midway between baffles by including them. The comparison with Figure 15b shows that the results are only marginally affected by this choice; levels of k increase slightly only near the blade edges in the lower impeller and remain practically unchanged elsewhere. Similar results are obtained for the other cases tested.

When SG simulations are conducted, the low-frequency terms are always implicitly taken into account by the time-dependent nature of the computation. However, the choice remains of whether including one-half of the time variance of the velocity in the computed turbulence energy k when this quantity is *visualized*, for example, in order to draw comparisons with experimental results. Again, all results discussed so far did not include the low-frequency terms; Figure 17b reports the turbulence energy distributions in a plane midway between baffles obtained for the case of diverging flow obtained by including them. By comparison with Figure 15c, only negligible changes in the distribution of k can be observed, mainly concentrated near the blade edges. Note that, when this latter simulation technique is used, the inclusion of the low-frequency terms can only lead to an *increase* in levels of k and by no means affects other computed quantities.

As a final comparison, Table 3 reports experimental and computed values of the *power number*, N_p. This is defined as $W/(\rho N^3 D^5)$, W being the dissipated power, ρ the fluid's density, N the rotational speed of the impellers (in rounds per second), and D their diameter. Both in the experiments and in the numerical simulations, W was determined to be the product of the resisting torque by the angular velocity. In experiments, the torque was directly measured; in the present numerical simulations, it was computed by summing the contributions due to (a) the pressure difference between the upstream and downstream faces of the baffles, and (b) the wall shear stress on the horizontal and lateral walls. This made it possible also to compute N_p from IBC simulations, in which, of course, the impeller region is *not* explicitly described.

The experimental value of N_p found for the parallel flow case is about twice the value most commonly reported in the literature for tanks stirred by *single* impellers; this confirms that the two impeller streams interact only weakly in this configuration. The measurements show that N_p decreases slightly in the diverging-flow case and more significantly in the merging-flow case, which also gave the shortest mixing time.

As expected, the trend just cited was correctly reproduced only by the SG or IO simulations. The former yielded values of N_p that were very close to those in the experiments in the parallel- and merging-flow configurations, and underestimated N_p more significantly ($\sim 10\%$) only in the diverging-flow case. IO results were proportional to the SG predictions, but $\sim 15\%$ lower. The IBC method underpredicted N_p severely in all cases and, of course, failed to predict its dependence upon the flow configuration.

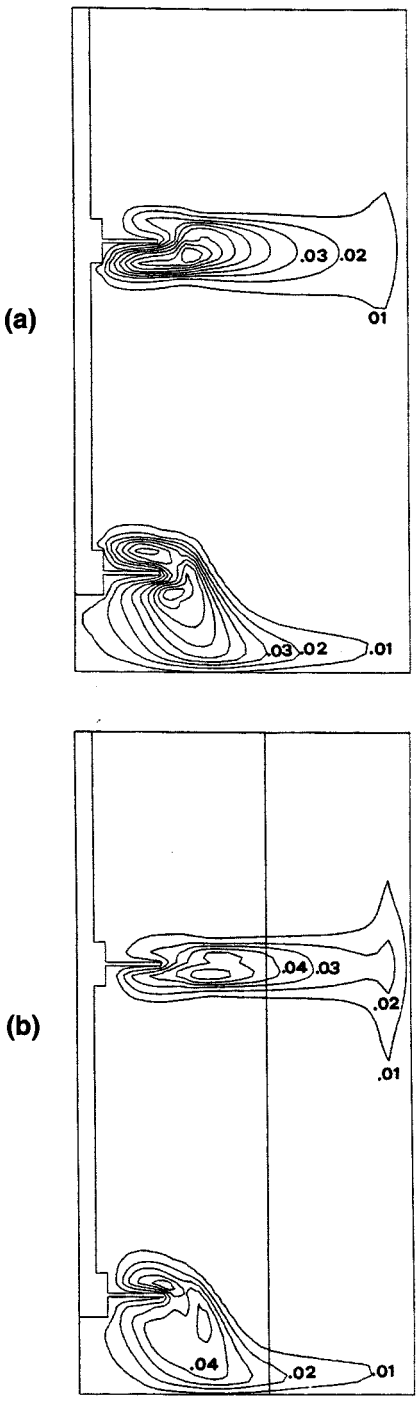

Figure 17. Turbulence energy distributions in a plane midway between baffles for the case of diverging flow obtained by including the low-frequency terms associated with the rotation of the impeller.

(a) IO predictions (compare with Figure 15b, obtained without low-frequency terms); (b) SG predictions (compare with Figure 15c, obtained without low-frequency terms).

To a certain extent, a similar comparison also can be made for the *flow number*, N_Q, defined for each impeller as $Q/(ND^3)$, in which Q is the volumetric flow rate discharged from the impeller and N, D are as defined previously. For the parallel-flow case, Rutherford et al. computed Q as:

$$Q = \int_{z_1}^{z_2} u_r \, 2\pi r \, dr, \tag{1}$$

in which the integration was performed for $r = D/2$ between the two axial locations z_1, z_2 at which the circumferentially-averaged radial velocity u_r vanished. With this definition, N_Q was found to be 0.76 for the lower impeller and 0.79 for the upper one. These figures are close to those usually reported in the literature for vessels stirred by single impellers. Values of N_Q were not reported for merging and diverging flow, since the presence of significant axial velocity components at the impeller's periphery makes the preceding definition of Q inappropriate in these cases.

Table 3. Power Number

Case	Experiments	IBC	IO	SG
A (parallel flow)	10.0	4.6	8.2	10.0
B (merging flow)	8.4	4.6	6.9	8.2
C (diverging flow)	9.5	4.5	7.1	8.4

For the same parallel-flow case and the same definition of Q, IO simulations gave values of N_Q of about 0.68 for both impellers (computed from the inner solution), with only a slight underprediction with respect to the experiments. For the sake of completeness, we also report that the values computed for the merging- and diverging-flow cases were 0.36 ~ 0.36 and 0.25 ~ 0.66 (lower ~ upper impeller), respectively.

SG predictions of N_Q were 0.72 ~ 0.72 (parallel flow), 0.29 ~ 0.29 (merging flow), and 0.29 ~ 0.72 (diverging flow) for the lower and upper impeller, respectively. Therefore, SG predictions were slightly higher than IO results (and closer to the experiments) for impeller flows that were mainly radial, but lower than IO results for impeller flows that had a strong axial component. This behavior is coherent with the fact that SG flow predictions exhibited a stronger axial component than IO results (see Figures 9c–9d and 13c–13d).

As regards IBC predictions, when this approach is used the flow number is an imposed, rather than a computed quantity, so the question of its prediction is meaningless.

Conclusions

Numerical predictions were obtained for the turbulent flow fields in a vessel stirred by a dual Rushton impeller. Three geometrical configurations were considered, for which published LDV results show that three markedly different flow patterns (parallel, merging, and diverging) develop.

Three alternative impeller modeling techniques were compared while using the same turbulence model, the same computer code and, essentially, the same numerical methods. Both the time-dependent sliding grid (SG) approach and the novel inner–outer (IO) technique satisfactorily reproduced the mean flow field and the distribution of turbulence energy for all three configurations. In the merging and diverging flow cases, the main discrepancy was the overprediction of the an-

gle formed by the flow issuing from the impeller with the horizontal; this is probably due to the inherent limitations of the k-ϵ turbulence model for flows with strong streamline curvature. The influence of the turbulence model in stirred-tank flow predictions is currently being investigated by our group.

In the merging and diverging configurations, the sliding-grid technique required a large number of impeller rotations to be simulated before converging to the correct, asymmetric solution, while shorter simulations (wrongly) predicted a parallel-flow pattern. On the other hand, the inner–outer method provided qualitatively correct flow patterns after only a few inner–outer iterations, further iterations providing only a quantitative refinement of the results.

A simpler impeller boundary conditions (IBC) modeling approach, based on experimental flow and turbulence data at the impeller's periphery obtained for a different single-impeller geometry, gave satisfactory results only in the simplest case of parallel flow, but failed to predict the effect of the relative position of the two impellers on the overall flow patterns. This confirms that the IBC approach can be useful only if (1) accurate flow data at the impeller boundaries are available for geometries close to that under consideration, or (2) the overall flow patterns in the vessel can be shown to be insensitive to the details of the flow at the impeller boundaries.

Acknowledgments

Funding from the Italian Ministry for University and Scientific Research (MURST 40% 1993–1994) is gratefully acknowledged. The authors thank Professor M. Yianneskis for his interest and advice. CFDS-FLOW3D is a proprietary code of AEA Technology at Harwell.

Literature Cited

AEA Technology, *CFDS-FLOW3D: User Guide*, Computational Fluid Dynamics Services, AEA Industrial Technology, Harwell, Oxon., UK (1994).

Bode, J., "Computational Fluid Dynamics Applications in the Chemical Industry," *Comput. Chem. Eng.*, **18**, S247 (1994).

Brucato, A., M. Ciofalo, F. Grisafi, and L. Rizzuti, "Application of a Numerical Fluid Dynamics Software to Stirred Tanks Modelling," *Supercomputing Tools for Science and Engineering*, D. Laforenza and R. Perego, eds., Franco Angeli, Milano, p. 413 (1989).

Brucato, A., M. Ciofalo, F. Grisafi, and L. Rizzuti, "Computer Simulation of Turbulent Fluid Flow in Baffled and Unbaffled Tanks Stirred by Radial Impellers," *Proc. Int. Conf. Computer Applications to Batch Processes*, V. G. Dovú, ed., Cengio, Italy, p. 69 (1990).

Brucato, A., M. Ciofalo, F. Grisafi, and G. Micale, "Complete Numerical Simulation of Flow Fields in Baffled Stirred Vessels: The Inner-Outer Approach," *Inst. Chem. Eng. Symp. Ser.*, **136**, 155 (1994).

Brucato, A., M. Ciofalo, F. Grisafi, and G. Micale, "Numerical Prediction of Flow Fields in Baffled Stirred Vessels: A Comparison of Alternative Modelling Approaches," *Chem. Eng. Sci.*, **53**, 3653 (1998).

Burns, A. D., and N. S. Wilkes, "A Finite-Difference Method for the Computation of Fluid Flows in Complex Three-Dimensional Geometries," *UKAEA Rep. AERE-R 12342*, Harwell, UK (1987).

Ciofalo, M., A. Brucato, F. Grisafi, and N. Torraca, "Turbulent Flow in Closed and Free-Surface Unbaffled Tanks Stirred by Radial Impellers," *Chem. Eng. Sci.*, **51**, 3557 (1996).

Daskopoulos, Ph., and C. K. Harris, "Three-Dimensional CFD Simulations of Turbulent Flow in Baffled Stirred Tanks: An Assessment of the Current Position," *Inst. Chem. Eng. Symp. Ser.*, **140**, 1 (1996).

Fokema, M. D., S. M. Kresta, and P. E. Wood, "Importance of Using the Correct Impeller Boundary Conditions for CFD Simulations of Stirred Tanks," *Can. J. Chem. Eng.*, **72**, 177 (1994).

Gosman, A. D., R. I. Issa, C. Lekakou, M. K. Looney, and S. Politis, "Multidimensional Modelling of Turbulent Two-Phase Flow in Stirred Vessels," *AIChE J.*, **38**, 1946 (1992).

Issa, R. I., "Full Field Computation of Mixing in Baffled Stirred Vessels," *Inst. Chem. Eng. Res. Event*, Birmingham, UK (1993).

Launder, B. E., and D. B. Spalding, "The Numerical Computation of Turbulent Flows," *Comput. Methods Appl. Mech. Eng.*, **3**, 269 (1974).

Luo, J. Y., A. D. Gosman, R. I. Issa, J. C. Middleton, and M. K. Fitzgerald, "Full Flow Field Computation of Mixing in Baffled Stirred Vessels," *Trans. Inst. Chem. Eng.*, **71**(A), 342 (1993).

Luo, J. Y., R. I. Issa, and A. D. Gosman, "Prediction of Impeller-Induced Flows in Mixing Vessels Using Multiple Frames of Reference," *Inst. Chem. Eng. Symp. Ser.*, **136**, 549 (1994).

Middleton, J. C., F. Pierce, and P. M. Lynch, "Computation of Flow Fields and Complex Reaction Yield in Turbulent Stirred Reactors and Comparison with Experimental Data," *Chem. Eng. Res. Des.*, **64**, 18 (1986).

Murthy, J. Y., S. R. Mathur, and D. Choudhury, "CFD Simulation of Flows in Stirred Tank Reactors Using a Sliding Mesh Technique," *Inst. Chem. Eng. Symp. Ser.*, **136**, 341 (1994).

Perng, C. Y., and J. Y. Murthy, "A Moving-Deforming Mesh Technique for Simulation of Flow in Mixing Tanks," *AIChE Symp. Ser.*, **89**(293), 37 (1993).

Ranade, V. V., and J. B. Joshi, "Flow Generated by Pitched Blade Turbines—I: Measurements Using Laser Doppler Anemometer; II: Simulation Using k-ϵ Model"(with A. G. Marathe), *Chem. Eng. Commun.*, **81**, 197 and 225 (1989).

Ranade, V. V., and J. B. Joshi, "Flow Generated by a Disc Turbine: Part I. Experimental; Part II. Mathematical Modelling and Comparison with Experimental Data," *Trans. Inst. Chem. Eng.*, **68**(A), 19 and 34 (1990).

Rhie, C. M., and W. L. Chow, "A Numerical Study of the Turbulent Flow Past an Aerofoil with Trailing Edge Separation," *AIAA J.*, **21**, 1525 (1983).

Rutherford, K., K. C. Lee, S. M. S. Mahmoudi, and M. Yianneskis, "Hydrodynamic Characteristics of Dual Rushton Impeller Stirred Vessels," *AIChE J.*, **42**(2), 332 (1996).

Tabor, G., A. D. Gosman, and R. Issa, "Numerical Simulation of the Flow in a Mixing Vessel Stirred by a Rushton Turbine," *Inst. Chem. Eng. Symp. Ser.*, **140**, 25 (1996).

Tatterson, G. B., *Scaleup and Design of Industrial Mixing Processes*, McGraw-Hill, New York (1994).

VanDoormal, J. P., and G. D. Raithby, "Enhancements of the SIMPLE Method for Predicting Incompressible Fluid Flows," *Numer. Heat Transfer*, **7**, 147 (1984).

Weetman, R. J., "Development of Transitional Flow Mixing Impeller," *Proc. Eur. Cong. Mixing*, Vol. 1, Bruges, Belgium, p. 25 (1991).

Wu, H., and G. K. Patterson, "Laser-Doppler Measurements of Turbulent-Flow Parameters in a Stirred Mixer," *Chem. Eng. Sci.*, **44**, 2207 (1989).

Manuscript received Oct. 7, 1997, and revision received Nov. 19, 1998.